UDC 538.4 : 532.526

FLOW OF A CONDUCTING FLUID PAST A CIRCULAR CYLINDER IN A TRANSVERSE MAGNETIC FIELD

Kh. E. Kalis, A. B. Tsinober, A. G. Shtern, and E. V. Shcherbinin

Magnitnaya Gidrodinamika, Vol. 1, No. 1, pp. 18-28, 1965

This paper presents the results of numerical calculations of magnetohydrodynamic flow around a circular cylinder, based on the exact Navier-Stokes equations, and a qualitative comparison of these results with experiments on the flow past cylinders of a conducting fluid in a transverse magnetic field. The calculations were made for Re = 40, since this is the number for which the flow calculations in ordinary hydrodynamics [1-3] were made. Although the experiments were conducted at considerably higher Reynolds numbers, a qualitative comparison still gives most interesting results.

1. Statement of problem

The problem is solved on the assumption that the magnetic field perturbations due to the motion of the fluid may be neglected as compared with the external magnetic field, in other words, the inductionless approximation is used.

In the dimensionless form, we may then write the equations of the problem as follows:

$$\begin{cases} (\mathbf{v}\,\mathrm{grad})\,\mathbf{v} = -\mathrm{grad}\,p + \dfrac{2}{\mathrm{Re}}\,\Delta\mathbf{v} + \dfrac{N}{2}[\mathbf{v}\times\mathbf{B}\times\mathbf{B} - \mathrm{grad}\,\varphi\times\mathbf{B}] \\ \mathrm{div}\,\mathbf{v} = 0 \\ \Delta\varphi = 0. \end{cases} \tag{1}$$

Here φ is the electric field potential, N is the magnetic interaction parameter, and the remaining symbols have the usual connotation.

In the first of Eqs. (1) the radius of the cylinder is taken as the characteristic length x, y, whereas in obtaining Re and N the diameter is retained as the characteristic dimension. The right side of the third equation is zero, since the flow in question is plane and the magnetic field is located in the plane of the flow. Therefore

$$\mathrm{div}\,(\mathbf{v}\times\mathbf{B}) = \mathbf{B}\,\mathrm{rot}\,\mathbf{v} - \mathbf{v}\,\mathrm{rot}\,\mathbf{B} \equiv 0.$$

In our case the magnetic field is perpendicular to the velocity of the free-stream flow. The cylinder is assumed to be insulated.

The boundary conditions have the following form:

1. For the velocity:

$$\begin{cases} u = v = 0 & \text{when } r = 1; \\ u = 1, \quad v = 0 & \text{when } r = \infty. \end{cases} \tag{2}$$

2. For the electric field potential:

$$\begin{cases} \dfrac{\partial\varphi}{\partial r} = 0 \\ \dfrac{\partial\varphi}{\partial r} = -\dfrac{\partial\varphi}{\partial z} + 1 = 0 \end{cases}$$

when r = 1, since at the surface of an insulated body the current normal to the surface is zero when r = ∞, since at infinity the total electric current is equal to zero. Here $r = \sqrt{x^2 + y^2}$. (3)

From the third of Eqs. (1) and the boundary conditions (3) it follows that correct to a constant

$$\varphi = z. \tag{4}$$

We shall introduce the stream function ψ and the curl of the velocity ζ:

$$u = \frac{\partial\Psi}{\partial y}; \quad v = -\frac{\partial\Psi}{\partial x}; \quad \zeta = \frac{\partial v}{\partial x} - \frac{\partial u}{\partial y} = -\Delta\Psi.$$

With (4) the first equation of system (1) reduces to the system:

$$\frac{2}{\mathrm{Re}}\Delta\zeta+\frac{D(\Psi,\zeta)}{D(x,y)}+\frac{\mathrm{N}}{2}\frac{\partial^2\Psi}{\partial y^2}=0;\quad \zeta=-\Delta\Psi.$$

It is convenient to introduce the perturbation of the stream function $\psi=\Psi-y$. Then the problem reduces to the solution of the system:

$$\begin{cases}\dfrac{2}{\mathrm{Re}}\Delta\zeta-\dfrac{\partial\zeta}{\partial x}+\dfrac{D(\psi,\zeta)}{D(x,y)}+\dfrac{\mathrm{N}}{2}\dfrac{\partial^2\psi}{\partial y^2}=0;\\ \zeta=-\Delta\psi\end{cases}\tag{5}$$

with boundary conditions $$1+\frac{\partial\psi}{\partial y}=\frac{\partial\psi}{\partial x}=0 \quad \text{when } r=1;$$

whence

$$\psi=\frac{\partial\psi}{\partial r}=-\sin\theta \text{ when } r=1.\tag{6}$$

Moreover, since the flow is symmetrical with respect to the x axis, $\dfrac{\partial u}{\partial y}=v=0$ when y = 0, we have

$$\begin{aligned}&\psi=\frac{\partial\psi}{\partial x}=0 \quad \text{when } y=0;\\ &\zeta=\frac{\partial\zeta}{\partial x}=0 \quad \text{when } y=0.\end{aligned}\tag{7}$$

Further

$$\zeta=\frac{\partial\zeta}{\partial x}=\frac{\partial\zeta}{\partial y}=0 \quad \text{when } y=\infty.$$

Expanding ψ in series with respect to r, from the second equation (5) for ζ at the surface of the cylinder we get

$$\zeta\Big|_{r=1}=-\frac{2}{(\Delta r)^2}\{\psi_{r=1+\Delta r}+\sin\theta(1+\Delta r)\}.\tag{8}$$

Condition (8) was first introduced by Thom [4].

Following Kawaguti [1], we shall map the exterior of the semicircle $1\le r<\infty$; $0\le\theta\le\pi$ onto the rectangle $0\le X\le 1$; $0\le Y\le 2$ with the aid of the transformation

$$X=\frac{1}{r};\quad Y=\frac{2}{\pi}\theta,\tag{9}$$

where $$r=\sqrt{x^2+y^2};\quad \theta=\operatorname{arctg}\frac{y}{x}.$$

Then, in the new coordinates, system (5) has the form

$$\begin{cases}\dfrac{2}{\mathrm{Re}}\left(X^4\dfrac{\partial^2\zeta}{\partial X^2}+\dfrac{4X^2}{\pi^2}\dfrac{\partial^2\zeta}{\partial Y^2}+X^3\dfrac{\partial\zeta}{\partial X}\right)+X^2\cos\dfrac{\pi}{2}Y\cdot\dfrac{\partial\zeta}{\partial X}+\\ +\dfrac{2X}{\pi}\sin\dfrac{\pi}{2}Y\cdot\dfrac{\partial\zeta}{\partial Y}-\dfrac{2X^3}{\pi}\dfrac{D(\psi,\zeta)}{D(X,Y)}+\\ +\dfrac{\mathrm{N}}{2}\left\{X^3\left(3\sin^2\dfrac{\pi}{2}Y-1\right)\dfrac{\partial\psi}{\partial X}+X^4\sin^2\dfrac{\pi}{2}Y\cdot\dfrac{\partial^2\psi}{\partial X^2}+\right.\\ \left.+\dfrac{4X}{\pi^2}\cos^2\dfrac{\pi}{2}Y\cdot\dfrac{\partial^2\psi}{\partial Y^2}-\dfrac{2X^3}{\pi}\sin\pi Y\cdot\dfrac{\partial^2\psi}{\partial X\partial Y}-\dfrac{2X^2}{\pi}\sin\pi Y\cdot\dfrac{\partial\psi}{\partial Y}\right\}=0;\\ \zeta=-X^4\dfrac{\partial^2\psi}{\partial X^2}+\dfrac{4X^2}{\pi^2}\dfrac{\partial^2\psi}{\partial Y^2}+X^3\dfrac{\partial\psi}{\partial X}\end{cases}\tag{10}$$

with boundary conditions

$$\psi=\zeta=0 \quad \text{when} \quad X=0,\quad Y=0 \text{ and } Y=2,$$

$$\psi=-\frac{\partial\psi}{\partial X}=-\sin\frac{\pi}{2}Y;\quad \zeta=-2\left[\frac{1}{h^2}\left\{\psi_{X=1-h}+(1+h)\sin\frac{\pi}{2}Y\right\}+\sin\frac{\pi}{2}Y\right];\quad \text{when } X=1;\tag{11}$$

where $h = \frac{\Delta r}{1+\Delta r}$ is the step with respect to the variable X.

2. Method of calculation

The solution of system (10) with boundary conditions (11) is sought as the limit as $t \to \infty$ of the solution of the corresponding nonstationary problem. The equations of the latter differ from those of the stationary case only in that on the right side of the first of Eqs. (10) zero is replaced by the derivative of ζ with respect to time, $\partial\zeta/\partial t$.

To pass from differential to finite-difference equations we used the following relations

$$\frac{\partial u}{\partial X} = \frac{u_{i+1,j} - u_{i-1,j}}{2h}; \qquad \frac{\partial u}{\partial Y} = \frac{u_{i,j+1} - u_{i,j-1}}{2l};$$

$$\frac{\partial^2 u}{\partial X^2} = \frac{u_{i+1,j} - 2u_{i,j} + u_{i-1,j}}{h^2}; \qquad \frac{\partial^2 u}{\partial Y^2} = \frac{u_{i,j+1} - 2u_{i,j} + u_{i,j-1}}{l^2};$$

$$\frac{\partial^2 u}{\partial X \partial Y} = \frac{u_{i+1,j+1} - u_{i-1,j+1} - u_{i+1,j-1} + u_{i-1,j-1}}{4hl};$$

$$\frac{\partial u}{\partial t} = \frac{u^{k+1} - u^k}{\tau},$$

where

$$u_{i,j} = \begin{cases} \psi_{ij} \\ \zeta_{ij} \end{cases}; \quad \begin{matrix} X_i = ih, & i = 0, 1, 2, \\ Y_j = jl, & j = 0, 1, 2, \\ t_k = k\tau, & k = 0, 1, 2 \ldots \end{matrix}$$

Here h, l, τ are the steps for X, Y, t, respectively.

Omitting the rather clumsy equation for the system of finite-difference equations, we shall merely note that this system was worked out by the difference factorization method [5]. As the initial approximation for N = 0 we took the fields ψ_{ij} and ζ_{ij} obtained by Kawaguti [1]. The calculations were continued until the process became stationary, i.e., $\partial\zeta/\partial t = 0$.

In practice, the calculations were continued up to t = 1-2 ($\tau = 1/32$), and interrupted for large values of N sooner than for small, since in this case the process becomes steady sooner. To test the reliability of the results, the case N = 0.2 was calculated a second time, using the values of ψ_{ij} and ζ_{ij} obtained for N = 4 as the initial approximation. The resulting values of ψ_{ij} and ζ_{ij} differed by less than 5% from the results obtained when the values of ψ_{ij} and ζ_{ij} calculated for N = 1/16 were used as the initial approximation.

Note that in computing the field of the curls at large distances from the cylinder (of the order of 7-10 radii) small positive values of the curl are obtained. For N = 0 these values did not exceed 0.01, but for N = 4 they reached 0.1. The appearance of these positive values of the curl is apparently due to the error resulting from the use of boundary condition (8). With increase in the interaction parameter N this error increases, since then at the surface of the cylinder the gradients of all the quantities (stream function, velocities, curls, etc.) increase.

Note further that system (5) can be treated as stationary from the very beginning. This is how Kawaguti [1] and Apelt [2] proceeded in calculating the ordinary hydrodynamic flow past a cylinder (i.e., N = 0) for Re = 40. However, ahead of the cylinder Kawaguti obtained strong oscillations of the function ζ, which at this point assumed very large positive values, though in fact this, does not make sense. Therefore in the region ahead of the body Kawaguti assumed $\zeta = 0$, as soon as positive values appeared in the calculating process. Of course, there is no mathematical justification for this. In Apelt's work [2] the calculations were performed in a finite region. At a distance of 20 radii the flow was assumed uniform. Note that at a distance of 10 radii positive values of the curl (of the order of 0.01) occurred.

We also attempted to calculate the stationary problem directly, but this attempt was not successful, since in the calculating process we encountered fluctuations of ζ analogous to those encountered by Kawaguti.

3. Results of the calculations

1. Streamline pattern. The streamlines were found from the field of the stream function $\Psi = y + \psi$ with the aid of a special program designed for finding the level lines of a given field of values of an arbitrary function.

Figure 1 shows the streamline patterns for different values of the interaction parameter N. As may be seen from the figure, the region of bound vortices behind the body contracts, the separation point moves back and starting from N = 0.5 the flow becomes separationless. Qualitatively, this is in good agreement with the experimental results. Figure 2 shows photos of the flow in the wake behind the cylinder taken from the surface of the mercury. A comparison of Fig. 1 with these photos reveals the known analogy in the change of the flow pattern with increase in N.

The difference due to the different values of the Re number used in the calculations and the experiments reduces to the fact that in the experiments, as the magnetic field intensity increases, the flow beyond the cylinder first loses the character of a Karman vortex street and degenerates into a pair of bound vortices; after this, however, the change in flow pattern is much the same in the experiments and in the calculations.

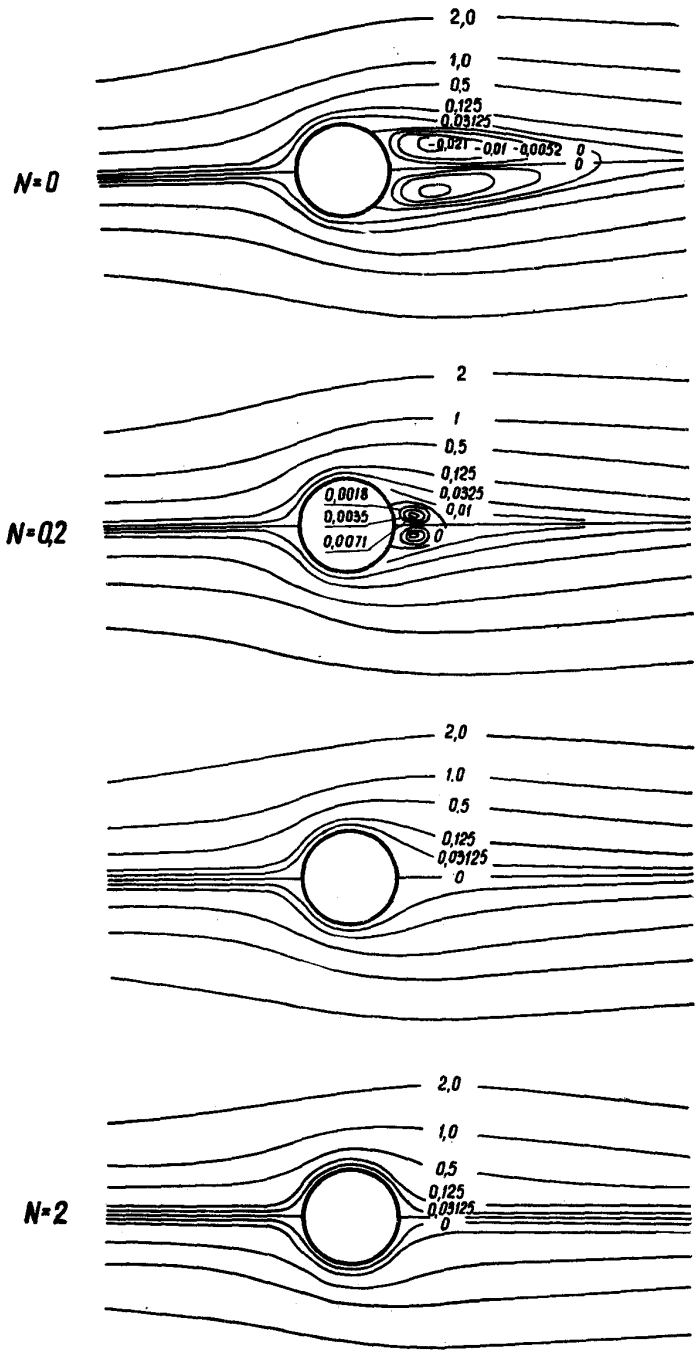

Fig. 1. Streamline pattern for flow of a conducting fluid past a circular cylinder in a transverse magnetic field for different values of N. Re = 40.

Both the calculations and the experiments show that there is a critical interaction parameter N_{cr} such that when $N \geq N_{cr}$ the flow of a conducting fluid past a circular cylinder (for $Re_m \ll 1$) becomes separationless. Clearly, N_{cr} is an increasing function of the Reynolds number, at least in the range of sufficiently small Re. In fact, when Re = 3-6, $N_{cr} = 0$;

however, calculations showed that when Re = 40, $N_{cr} = 0.5$; experiments [6], carried out at Re = 10^3-10^4, gave $N_{cr} \sim 1$-2. It may be expected that this value of N_{cr} is close to the limit to which $N_{cr} = f(Re)$ tends with increase in Re. However, if the cylinder is not electrically insulated from the external flow, then as experiments [6] showed, the value of N_{cr} still depends on the conductivity of the cylinder itself as well.

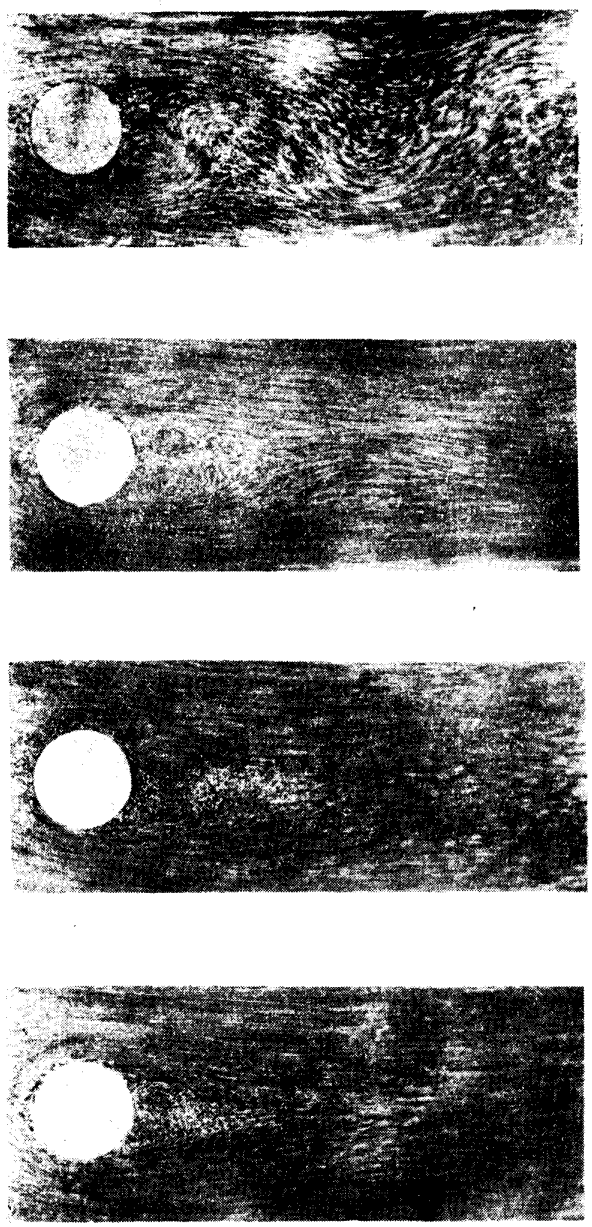

Fig. 2. Photographs of the flow behind a circular cylinder for different interaction parameters N. Re = 8200.

From the above streamline patterns it is also clear that as N increases the streamlines contract toward the cylinder, the field acting more strongly on those streamlines that lie closer to the cylinder surface.

Figure 3 shows the velocity along the x axis as a function of the distance from the surface of the cylinder. The solid lines correspond to the velocities ahead of the cylinder, the broken lines to the velocities in the wake behind the cylinder. As might be expected, as the distance from the body increases, the velocity approaches its value for the free-stream flow the more rapidly the greater the interaction parameter.

2. Distribution of curl of velocity. The lines of constant curl were found from the curl field in the same way as the streamlines were found from the field of the stream function Ψ. Figure 4 shows the lines of constant curl for several values of N. Here it is also clear that the influence of the magnetic field is strongest in the immediate vicinity of the surface and in the wake of the cylinder.

Figure 5 shows the distribution of the curl of the velocity over the surface of the cylinder. Correct to the coefficient, this coincides with the distribution of the friction forces, since

$$\zeta_{r=1} = \left.\frac{\partial v_\theta}{\partial r}\right|_{r=1}.$$

It is clear that with increase in N the friction forces at the surface increase and, starting with N = 0.5, i.e., from the moment of transition to separationless flow, have everywhere the same direction.

3. Pressure distribution over surface of cylinder. The pressure distribution is computed from the steady-state equations (1). In order to find $p(1, \theta)$, we first find the value of $p(1, \pi)$ from Eqs. (1) written in polar coordinates.

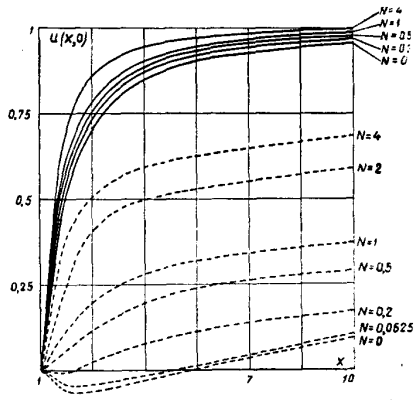

Fig. 3. Velocity distribution along the x axis for different values of N. Re = 40.

Integrating this equation along the zero streamline $\theta = \pi$, and over to the coordinates X and Y, we get

$$p(1,\pi) = \frac{4}{\pi \mathrm{Re}}\int_0^1 \frac{1}{X}\frac{\partial \zeta}{\partial Y}\,dX + \frac{N}{\pi}\int_0^1 \frac{1}{X}\frac{\partial \psi}{\partial Y}\,dX + \frac{1}{2}.$$

(Here $p(\infty, \pi) = 0$, since the pressure is determined up to an arbitary additive constant.) Then $p(1, \theta)$ is determined by integrating Eq. (1) along the surface of the cylinder (r = 1):

$$p(1,\theta) = p(1,\pi) + \frac{\pi}{\mathrm{Re}}\int_Y^2 \frac{\partial \zeta}{\partial X}\,dY + \frac{N}{2}\left(\cos\frac{\pi Y}{2} + 1\right).$$

From this formula, using the obtained fields of ψ and ζ, we calculate the pressure distribution over the surface of the cylinder $p(1, \theta)$.

Figure 6 shows the pressure distribution calculated in this way for several values of N. Clearly, with increase in N the pressure ahead of the cylinder increases considerably, the coefficient of the pressure at the forward stagnation point being much greater than unity. The same figure shows the pressure distribution curves obtained experimentally for Re = 3120. Although different Reynolds numbers were used in the calculations and in the experiment, the two sets of results are qualitatively in good agreement. For the forward stagnation point they also coincide quantitatively, as may be seen from Fig. 7, which shows the dependence of the pressure coefficient at the forward stagnation point on $N^{2/3}$. Starting from N = 1, this curve practically coincides with the straight line $1 + 3N^{2/3}/2$, which corresponds to the asymptotic expression obtained in [7] for the pressure at the forward stagnation point in the case of large N:

$$2\Delta p/\rho U^2 \sim 1 + kN^{2/3}.$$

Figure 7 also presents a graph with the results of measurements of the pressure at the forward stagnation point for Re ~ 10^3-10^4. It is easy to see that these are correlated by the same relation to which the calculated points tend asymptotically.

Over the rear part of the cylinder the pressure decreases, the point of minimum pressure moving downwards with respect to the flow; at $N \geq 2$ it meets the rear stagnation point.

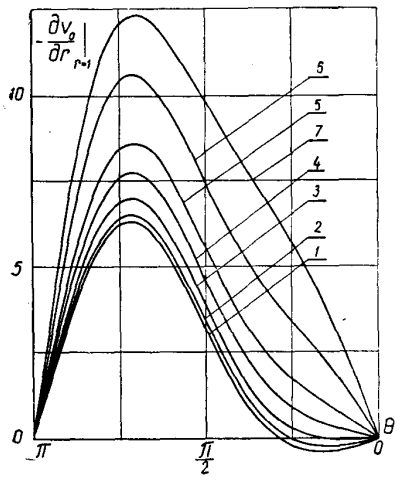

Fig. 5. Distribution of friction forces over the surface of a circular cylinder for different values of N. Re = 40. 1) N = 0, 2) N = 1/16, 3) N = 0.2, 4) N = 0.5, 5) N = 1, 6) N = 2, 7) N = 4.

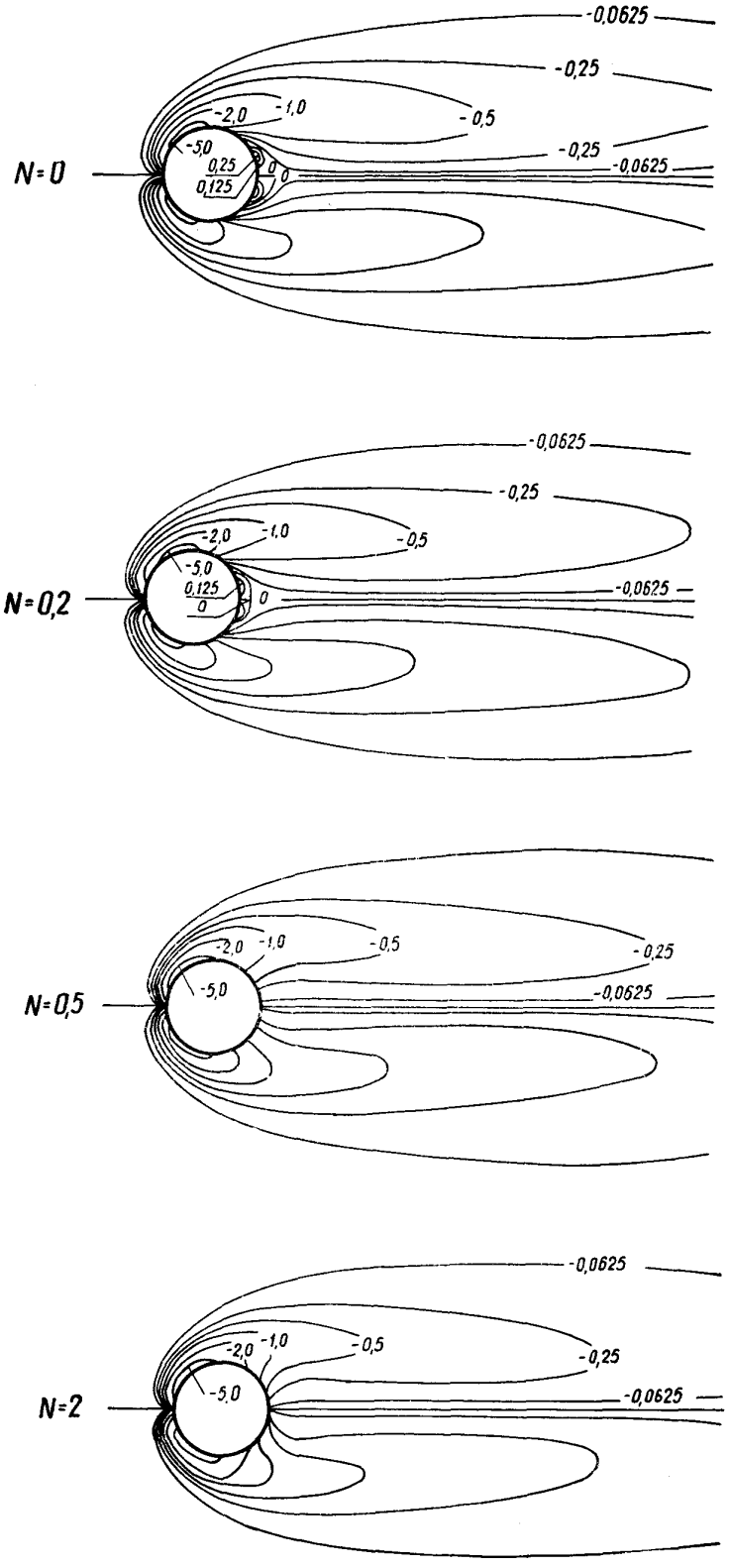

Fig. 4. Constant curl lines for different values of N. Re = 40.

4. Drag coefficient C_x. The drag force for flow past a cylinder is given by

$$F = -\int_0^{2\pi} p(1,\theta)\cos\theta d\theta - \rho\nu\int_0^{2\pi}\zeta(1,\theta)\sin\theta d\theta,$$

where the first term corresponds to the form drag and the second to the friction drag. From this expression, using formula (9), for the drag coefficient we get

$$C_x = -\pi\int_0^2 p(1,Y)\cos\frac{\pi}{2}YdY - \frac{2\pi}{\mathrm{Re}}\int_0^2\zeta(1,Y)\sin\frac{\pi}{2}YdY.$$

Figure 8 shows the total drag, form drag, and friction drag as a function of N.

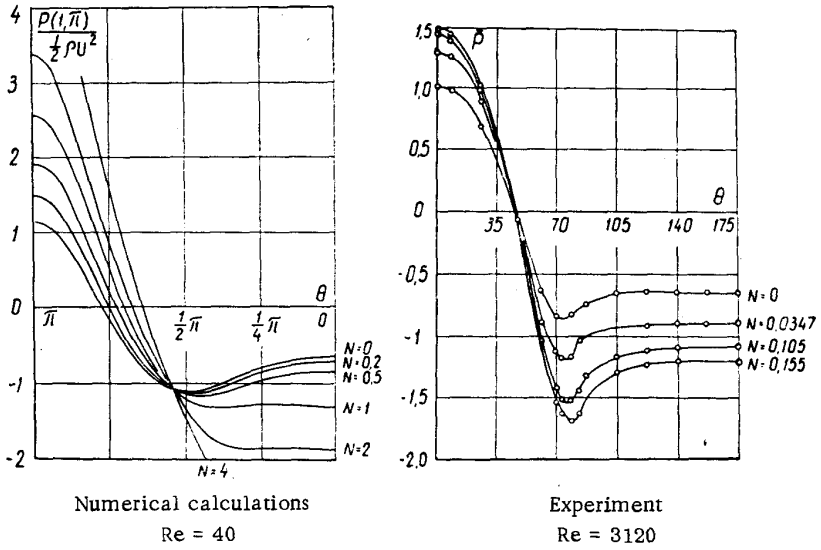

Numerical calculations
Re = 40

Experiment
Re = 3120

Fig. 6. Pressure distribution over the surface of a circular cylinder for different values of N.

It is clear that in a magnetic field the resistance of the cylinder sharply increases. Thus, for N = 4 the drag coefficient reaches a value $C_x = 7.14$, whereas for N = 0, $C_x = 1.645$.

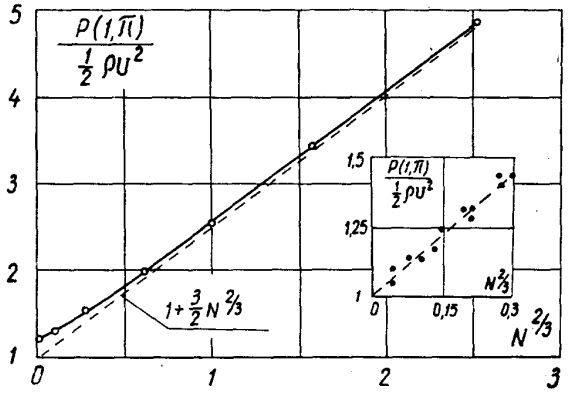

Fig. 7. Pressure coefficient at the forward stagnation point as a function of N.

Note that when N = 0 the values of C_{x0}, C_{p0}, and C_{f0} are in good agreement with the results obtained by Kawaguti [1] and Apelt [2], as may be seen from the table. It should also be noted that an analogous increase in the resistance of a cylinder in a magnetic field is also observed experimentally at high Reynolds numbers [8].

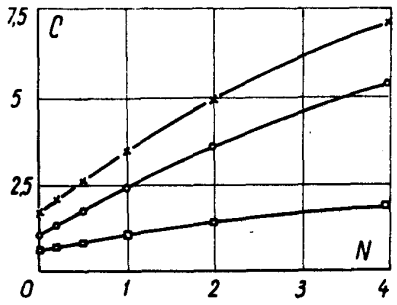

Fig. 8. Drag coefficient of a circular cylinder as a function of N. Re = 40.
X – $C_x = C_p + C_f$, total drag,
O – C_p, form drag
□ – C_f, friction drag

Source	C_{x_0}	C_{p_0}	C_{f_0}
Kawaguti	1.618	1.053	0.565
Apelt	1.469	0.928	0.568
Our calculations	1.645	1.0597	0.585

REFERENCES

1. M. Kawaguti, Journ. Phys. Soc. Japan, 8, 6, 1953.
2. C. J. Apelt, ARC Repts and Mem., 3175, 1961.
3. A. Thom and C. Apelt, Field Computations in Engineering and Physics [Russian translation], Moscow, 1964.
4. A. Thom, Proc. Roy. Soc., A141, 651, 1933.
5. I. S. Berezin and I. N. Zhidkov, Methods of Computation [in Russian], 2, GIFML, 1962.
6. A. B. Tsinober, A. G. Shtern, and E. V. Scherbinin, Izv. AN LatvSSR, 12, 49, 1963.
7. A. B. Tsinober, A. G. Shtern, and E. V. Scherbinin, Izv. AN LatvSSR, ser. fiz. i tekhn. nauk, 4, 31, 1964.
8. A. B. Tsinober and E. V. Shcherbinin, Izv. AN LatvSSR, 11, 45, 1962.

15 September 1964